Proceedings of the 21st ICSMGE, Vienna, Austria, 14 – 19 June 2026. Pistrol, Adam & Schweiger (eds.)
Published by: ÖGG, Austrian Society for Geomechanics, Salzburg, Austria, ISBN 978-3-9503898-4-5
https://doi.org/10.53243/ICSMGE2026-1739

Analytical seismic fragility curves for a tailings dam in Chile

César Pastén, Agustín Meriño, Pablo Heresi
Department of Civil Engineering, University of Chile, Chile, cpasten@uchile.cl

ABSTRACT: The adoption of the Performance-Based Earthquake Engineering (PBEE) framework can support stakeholders' seismic risk decision-making for tailings storage facility (TSF) projects in Chile, where large megathrust earthquakes are the main natural hazard that controls their designs. TSFs can impound millions of cubic meters of tailings supported by large earth dams that can reach hundreds of meters in height, following a construction process that can last several decades. The adoption of PBEE requires the definition of fragility curves to estimate the conditional probability of exceeding a given damage state, given a seismic intensity measure (IM), such as peak ground acceleration or peak ground velocity. Archetypal cross-sections of Chilean tailings earth dams of 50 m and 100 m height and various downstream slopes modelled with a nonlinear constitutive model were subjected to a set of ground motions of large Chilean earthquakes, adopting a cloud analysis, using the PLAXIS2D software. The settlement of the dam crest was considered as the engineering demand parameter (EDP), and the optimized average spectral acceleration resulted in the most efficient IM. Numerical simulations allowed defining analytical fragility curves for various damage states. Results show that the probability of damage increases as the downstream slope becomes steeper.

KEYWORDS: Tailings dams, seismic fragility curves.

1 INTRODUCTION

The design of tailings dams in Chile is prescribed by the Supreme Decree Nº248 (MMC, 2007) and the Decree 50 (MOP, 2015), both of which require pseudo-static limit equilibrium and dynamic analyses to verify the seismic stability of the dam when subjected to earthquake loadings. The dynamic analyses confirm that the seismically-induced dam deformation does not compromise the safe containment of tailings. The input ground motions adopted in these analyses, either synthetic or instrumental records, are selected to be compatible with results from site-specific seismic hazard analyses. These ground motions can be characterized by intensity measures (IM), such as peak ground acceleration (PGA), peak ground velocity (PGV), Arias Intensity (AI), destructiveness potential (P_d), cumulative absolute velocity (CAV), and pseudo-spectral accelerations at a given period [Sa(T)].

The performance-based earthquake engineering (PBEE) framework aims to determine the probability of observing structural damage given an IM at the site where the structure is emplaced. Our long-term project seeks to adopt the PBEE framework for tailings dams in Chile, given the main characteristics of the dams and the seismotectonic framework. One of the steps in the adoption process is to find an engineering demand parameter (EDP), defined as a structural response quantity that can be used to estimate the failure or damage state of a component. Depending on the analyzed structure, there may be several EDPs that can be correlated with damage. The EDP is selected such that it can be easily estimated from a known IM, which is usually determined from site-specific seismic hazard analyses. The deformation of the dam at specific locations, such as crest settlement and downstream slope lateral displacement, can be considered as EDPs. Efficiency is the ability of a given IM to estimate the EDP with low uncertainty.

Several studies have determined the most efficient IMs for predictions of EDPs in geotechnical structures with the aid of nonlinear dynamic finite element analyses. Armstrong et al. (2020) modeled two earthfill dams and executed 342 simulations to find that the most efficient IM that predicts accumulated vertical and horizontal crest displacements was the AI. Labanda et al. (2021) built a representative tailings dam model following the upstream method (currently banned in Chile), including materials susceptible to liquefaction, and executed 25 simulations, finding that the most efficient IM was the spectral power of the seismic record in a frequency band related to the predominant frequency of the analyzed dam. Cho & Rathje (2022) analyzed 49 uniform material slope models of 15 and 30 m height and performed 1051 simulations for each model, to find that the PGV was the most efficient IM. Boada et al. (2023) analyzed abandoned tailings dams, consisting of a uniform material slope of 15 m height, subjected to 169 strong ground motions, and found that the most efficient IM was AI.

This paper focuses on analyzing through numerical simulations the efficiency of various IMs and EDPs for archetypes of Chilean tailings dams constructed with borrowed materials. Combining results from efficiency and various capacity models, fragility curves are proposed for the analyzed archetypes.

2 NUMERICAL SIMULATIONS

2.1 *Numerical model*

The geometry of the archetypes of Chilean tailings dams analyzed in this paper is schematically depicted in Figure 1. The dams are 50 and 100 m height, with constant upstream slopes of H:V= 2.0:1.0, 15 m of crest width, and 5 m freeboard. We analyzed three downstream slopes of H:V= 1.8:1.0, 2.0:1.0, and 2.2:1.0, and two dam material stiffnesses.

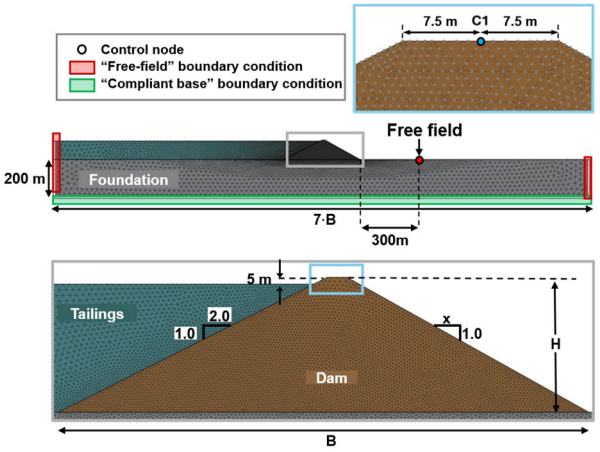

Figure 1. Numerical model of archetype tailings dam.

Based on the geometry in Figure 1, finite-element method (FEM) models were developed with the PLAXIS2D software (Plaxis, 2022). The numerical models consist of three materials: the embankment dam, the stored tailings, and the foundation

soil (Figure 1). The materials were assumed to be fully bonded, and the interface was not explicitly modeled. Although this assumption may influence the dynamic displacement pattern, it significantly reduces computational cost. The constitutive models adopted for each material were the Hardening Soil with Small Strain Stiffness (HSS), the Mohr-Coulomb (MC), and the Linear Elastic (LE) models, respectively. The HSS model is the simplest elastoplastic nonlinear model implemented in the PLAXIS2D software that can account for stiffness degradation and hysteretic damping of granular materials. The constitutive model parameters of the dam material are shown in Table 1.

The elastoplastic MC model was chosen for simplicity, given the large number of simulations, as well as the selection of the LE model for the foundation. The model parameters for these two materials are shown in Tables 2 and 3.

Table 1. Embankment dam parameters - HSS model.

Parameter	Symbol	Value	Unit
Total unit weight	γ	20	kN/m^3
Secant stiffness in standard drained triaxial test	E_{50}^{ref}	30	MPa
Tangent stiffness for primary oedometer loading	E_{eod}^{ref}	30	MPa
Unloading/reloading stiffness from drained triaxial test	E_{ur}^{ref}	90	MPa
Power for stress-level dependency of stiffness	M	0.46	-
Cohesion	c'	10	kPa
Friction angle	φ'	39	°
Dilatancy angle	ψ'	0	°
Poisson's ratio for unloading-reloading	ν_{ur}	0.2	-
Failure ratio	R_f	0.9	-
Reference mean pressure	p_{ref}	100	kPa
Reference shear modulus at very small strains	G_0^{ref}	165 – 330	MPa
Threshold shear strain at which G_s=0.722·G_0	$\gamma_{0.7}$	0.3	-

Table 2. Tailings parameters – MC model.

Parameter	Symbol	Value	Unit
Total unit weight	γ	17	kN/m^3
Young's modulus	E	7.8	MPa
Cohesion	c'	20	kPa
Increase of cohesion with depth	c'_{inc}	1.7	kPa/m
Friction angle	φ'	0	°
Dilatancy angle	ψ'	0	°
Poisson's ratio	ν	0.4	-

Table 3. Foundation parameters – LE model.

Parameter	Symbol	Value	Unit
Total unit weight	γ	24	kN/m^3
Young's modulus	E	8450	MPa
Poisson's ratio	ν	0.2	-

The dam stiffness was controlled by the small-strain parameter G_0^{ref}. We selected two values to represent a range of material stiffness: (1) G_0^{ref} = 165 MPa, which represents a material with average stiffness; and (2) G_0^{ref} = 330 MPa, which represents a stiffer material. The adopted parameters result in a shear modulus increasing with depth from the dam crest. The shear wave velocity normalized at 100 kPa of effective vertical stress (Vs_1) in the dams' central axes are 284 m/s and 402 m/s for the average and high stiffness cases, respectively.

The yield seismic coefficients (Ky) obtained from limit equilibrium (LEM) analyses for each archetype dam are shown in Table 5.

Table 4. Dams yield seismic coefficients Ky.

Downstream slope (H:V)	H = 50 m	H = 100 m
1.8:1.0	0.277	0.238
2.0:1.0	0.322	0.281
2.2:1.0	0.355	0.318

The model foundation material was chosen to have a high stiffness (Vs= 1200 m/s) since many of the tailings dams constructed in northern Chile are founded on stiff soils. Assuming a rigid and elastic foundation reduces radiation damping from the dam, which could exaggerate displacement predictions. The finite element sizes were defined such that the maximum transmitted shear wave frequency in the archetype models is 25 Hz, according to recommendations from Kuhlemeyer & Lysmer (1973).

2.2 *Input Ground Motions*

Dynamic numerical simulations of the seismic response of each archetype dam were performed considering 14 input ground motions, corresponding to a selected set of records from three Chilean megathrust earthquakes: (1) the 2010 Mw 8.8 Maule Earthquake; (2) the 2014 Mw 8.3 Iquique Earthquake; and (3) the 2015 Mw 8.4 Illapel Earthquake. The selected ground motions, shown in Table 5, simultaneously satisfy two conditions: (1) the station's average shear-wave velocity from the surface to a depth of 30 m (Vs_{30}) is larger than 750 m/s; and (2) the recorded peak ground acceleration (PGA) is larger than 0.12 g. Ground motions were scaled by 1.0, 1.25, 1.5, 1.75 and 2.0 to enlarge the database and increase the shaking intensities. Due to wave amplification in the foundation material, the ground motions calculated at the model free-field monitoring point (see Figure 1) were amplified. Those records that reached PGA > 1.2 g or PGV > 1 m/s at the free-field control were removed from the analysis. Results in the following sections account for a total of 57 ground motions.

Table 5. Ground motion records.

Earthquake	Station	Component	PGA (g)
2015 Illapel	CO06	NS-EW	0.35-0.33
2014 Iquique	PB11	NS-EW	0.57-0.50
2014 Iquique	PSGCX	EW	0.17
2014 Iquique	T08A	EW	0.42
2010 Maule	Rapel	NS-EW	0.17-0.19
2010 Maule	Santa Lucía	NS	0.25
2010 Maule	Melado	EW	0.13
2010 Maule	El Roble	NS-EW	0.18-0.13
2010 Maule	Convento Viejo	NS-EW	0.16-0.15

3 EFFICIENCY

The vertical displacement (settlement) of the control node in center of the dam crest (point C1 in Figure 1) was plotted against different IMs calculated in the free-field control point. Figure 2 shows the vertical displacement of the dam crest as a function of the optimized average spectral acceleration, Sa_{avg_opt}, for four dam archetypes. The average spectral acceleration Sa_{avg} is defined as (Eads et al. 2015):

$$Sa_{avg}(T_a, T_b) = \left[\prod_{i=1}^{N} Sa(T_i)\right]^{1/N} \quad (1)$$

where N is the number of considered spectral ordinates, and the periods T_i range from $T_1 = T_a$ to $T_N = T_b$. In this study, Sa_{avg_opt} is Sa_{avg} calculated over the period range $T_a = 0.1$ s to $T_b = 0.75$ s, with a spacing of 0.01 s. These values of T_a and T_b were selected to maximize the mean efficiency for predicting vertical crest displacements in the twelve dam archetypes analyzed in this study.

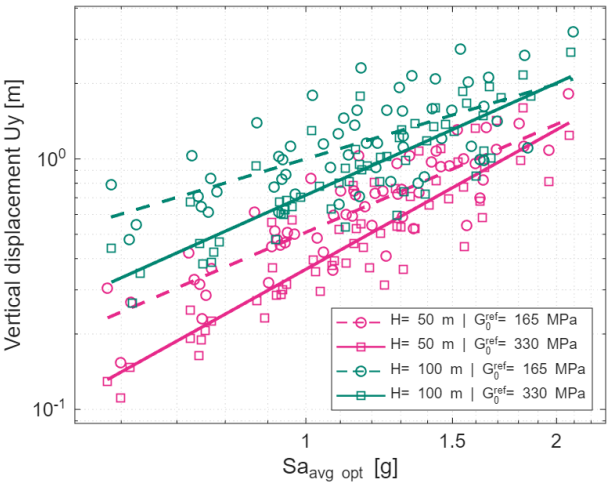

Figure 2. Vertical displacement of the dam crests as a function of Sa_{avg_opt} for dam archetypes with downstream slopes H:V = 2.0:1.0.

The efficiency of different IMs was evaluated with the residual standard deviation of the linear regression between the natural logarithms of U_y and IM, as follows:

$$\sigma_{U_y|IM} = \sqrt{\frac{\sum_{i=1}^{n}\left(U_y - U_y^p\right)^2}{n-2}} \quad (2)$$

Where n is the number of simulations for each archetype, U_y is the crest settlement obtained in the simulations and U_y^p is the predicted settlement as a function of the IM, given by:

$$ln\left(U_y^p\right) = a_{1\_IM} + a_{2\_IM} \cdot ln(IM) \quad (3)$$

where a_{i_IM} are coefficients determined through a linear regression analysis.

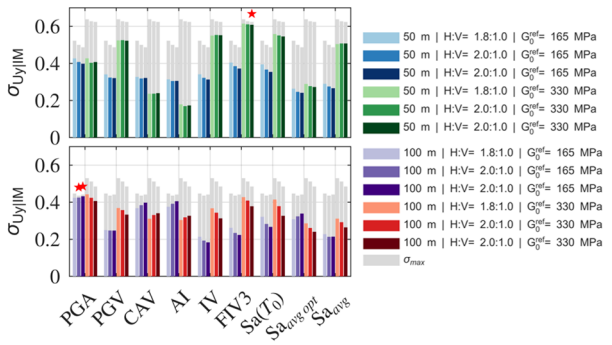

Figure 3. Efficiency of various IMs to predict vertical crest displacement (settlement). σ_{max} is the standard deviation of the numerically obtained vertical displacements for each dam archetype and stars on top of some IMs represent statistically insignificant regressions (p-values > 0.05).

Figure 3 shows the residual standard deviation of nine differrent IMs, including the PGA, PGV, CAV, AI, the incremental velocity (IV), the filtered incremental velocity (FIV3), the spectral acceleration at the fundamental period of the dams [$Sa(T_0)$], Sa_{avg_opt}, and the average spectral acceleration Sa_{avg}. The selected IM was Sa_{avg_opt}, which is highly efficient, i.e., exhibites low residual standard deviation across all dam archetypes, it can be readily estimated from existing ground motion models for Sa(T), and it is sufficient relative to other IMs (the corresponding analysis is omitted due to space limitations).

4 CAPACITY MODEL

The adopted capacity models are those for moderate and severe damage of He & Rathje (2024), defined in terms of relative crest settlement. In addition, we defined a damage state considering the freeboard of the models. The median of this damage state was set such that it corresponds to half the freeboard of the models (2.5 m), and the standard deviation was defined to be equal to that of the severe damage state. Figure 4 shows the probability of exceeding different damage states as a function of the crest vertical displacement for different capacity models.

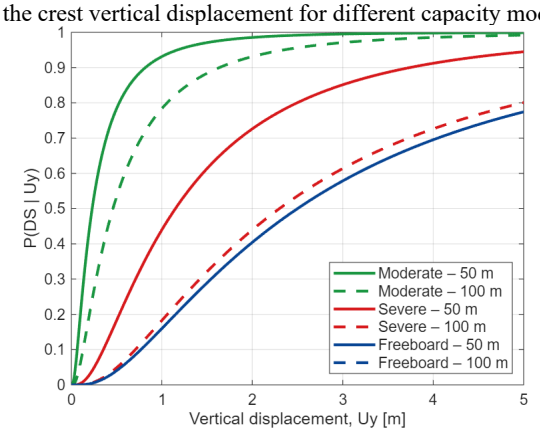

Figure 4. Capacity models. Moderate and severe damage states are defined in He & Rathje (2024).

5 FRAGILITY CURVES

The fragility curves $P(DS \mid Sa_{avg\_opt})$, describing the probability of exceeding a given damage state conditioned on a value of Sa_{avg_opt}, were calculated as follows:

$$P\left(DS|Sa_{avg\_opt}\right) = \int P\left(DS|U_y\right) \cdot f_{U_y}\left(u_y|Sa_{avg\_opt}\right) \cdot d\left(u_y\right) \quad (2)$$

where $P(DS \mid U_y)$ is the probability of exceeding a given damage state conditioned on a value of U_y (Figure 4), and $f_{Uy}(u_y \mid Sa_{avg\_opt})$ is the probability density function of U_y conditioned on a ground motion intensity Sa_{avg_opt} (obtained from Figure 2).

Figure 5 shows examples of fragility curves for 50 m height dams with various downstream slopes and $G_0^{ref} = 165$ MPa. The moderate damage state is quickly attained for $Sa_{avg\_opt} > 0.1$ g, whereas the damage state associated to the freeboard starts to develop for $Sa_{avg\_opt} > 0.5$ g. Steeper downstream slopes have higher damage probabilities.

The medians of the fragility curves for 50 m and 100 m height dams are shown in Figures 6 and 7, respectively. The medians increase with the downstream slope, regardless of the capacity model and damage state. Stiffer models have higher means, considering the He and Rathje moderate damage state. In contrast, the medians of the stiffer models are lower considering the freeboard damage state.

The standard deviations of fragility curves β for 50 m height dams (Figure 6) remain relatively insensitive to the

downstream slope. In general, stiffer models have lower standard deviations (Figures 6 and 7).

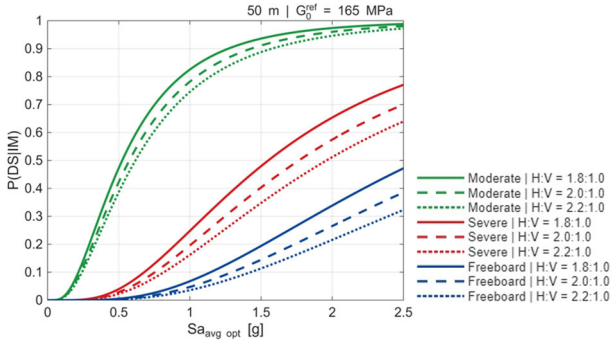

Figure 5. Fragility curves for 50 m height dams with various downstream slopes and G_0^{ref} = 165 MPa.

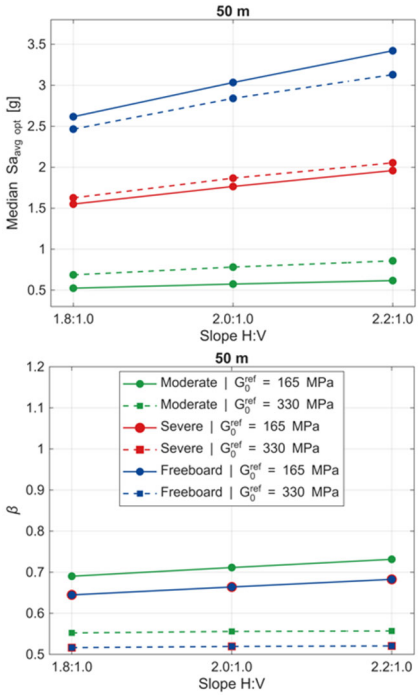

Figure 6. Parameters of the fragility curves for 50 m height dams. Squares joined with dotted lines are stiffer models (G_0^{ref}= 330 MPa).

6 CONCLUSIONS

Analytical seismic fragility curves were developed for earth-fill tailings dams in Chile based on numerical simulations of dam archetypes subjected to seismic records of large Chilean megathrust earthquakes, following the PBEE framework. The curves were conditioned on the Sa_{avg_opt}, which can be easily estimated using readily available ground motion models in seismic hazard analyses.

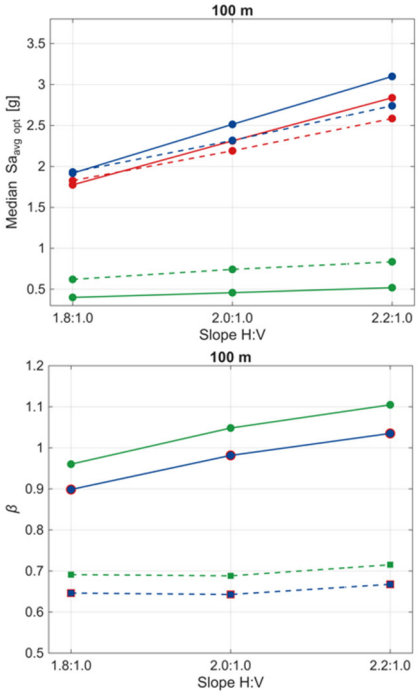

Figure 7. Parameters of the fragility curves for 100 m height dams. Squares joined with dotted lines are stiffer models (G_0^{ref}= 330 MPa).

7 ACKNOWLEDGEMENTS

Funding for this research was provided by ANID projects FONDECYT Nº1240744 and AMTC Basal Project AFB230001.

8 REFERENCES

Armstrong, R., Kishida, T., and Park, D. 2020. Efficiency of ground motion intensity measures with earthquake-induced earth dam deformations. *Earthquake Spectra* 37(1), 5-25.

Boada, G., Pastén, C., and Heresi, P. 2023. Analytical fragility curves for abandoned tailings dams in North-Central Chile. *Soil Dynamics and Earthquake Engineering* 164, 107637.

Cho, Y. and Rathje, E.M. 2022. Generic Predictive Model of Earthquake-Induced Slope Displacements Derived from Finite-Element Analysis. *Journal of Geotechnical and Geoenvironmental Engineering* 148(4), 04022010.

Eads, L., Miranda, E., and Lignos, D.G. 2015. Average spectral acceleration as an intensity measure for collapse risk assessment. *Earthquake Engineering & Structural Dynamics* 44(12), 2057-2073.

Kuhlemeyer, R., and Lysmer, J. 1973. Finite element method accuracy for wave propagation problems. *Journal of the Soil Mechanics and Foundations Division* 99(5), 421-427.

He, J., and Rathje, E.M. 2024. Seismic capacity models for earth dams and their use in developing fragility curves. *Earthquake Spectra* 40(3), 1986-2007.

Labanda, N., Sottile, M., Cueto, I., and Sfriso, A. 2021. Screening of seismic records to perform time-history dynamic analyses of tailings dams: a power-spectral based approach, *Soil Dynamics and Earthquake Engineering* 146, 106750.

MMC. 2007. Decreto Supremo N°248: Reglamento para la aprobación de Proyectos de Diseño, Construcción, Operación y Cierre de los Depósitos de Relaves. Ministerio de Minería, Chile.

MOP. 2015. Decreto 50: Aprueba reglamento a que se refiere el artículo 295 inciso 2º, del código de aguas, estableciendo las condiciones técnicas que deberán cumplirse en el proyecto, construcción y operación de las obras hidráulicas identificadas en el artículo 294 del referido texto legal. Ministerio de Obras Públicas, Chile.

Plaxis. 2022. PLAXIS 2D Reference Manual. Dublin: Bentley Systems International Limited.